Available online at www.sciencedirect.com

ScienceDirect

Acta Materialia 85 (2015) 53–66

Acta MATERIALIA

www.elsevier.com/locate/actamat

Computationally efficient and quantitatively accurate multiscale simulation of solid-solution strengthening by ab initio calculation

Duancheng Ma,[a,*] Martin Friák,[a,b] Johann von Pezold,[a] Dierk Raabe[a] and Jörg Neugebauer[a]

[a] *Max-Planck-Institut für Eisenforschung, Max-Planck-Str. 1, 40237 Düsseldorf, Germany*

[b] *Institute of Physics of Materials, Academy of Sciences of the Czech Republic, v.v.i, Zi zkova 22, Brno, Czech Republic*

Received 26 July 2014; revised 17 October 2014; accepted 20 October 2014

Abstract—We propose an approach for the computationally efficient and quantitatively accurate prediction of solid-solution strengthening. It combines the 2-D Peierls–Nabarro model and a recently developed solid-solution strengthening model. Solid-solution strengthening is examined with Al–Mg and Al–Li as representative alloy systems, demonstrating a good agreement between theory and experiments within the temperature range in which the dislocation motion is overdamped. Through a parametric study, two guideline maps of the misfit parameters against (i) the critical resolved shear stress, τ_0, at 0 K and (ii) the energy barrier, ΔE_b, against dislocation motion in a solid solution with randomly distributed solute atoms are created. With these two guideline maps, τ_0 at finite temperatures is predicted for other Al binary systems, and compared with available experiments, achieving good agreement.

Keywords: Solid-solution strengthening; DFT; Peierls–Nabarro model; Ab initio; Al alloys

1. Introduction

By using ab initio methods, two kinds of approaches are usually employed to simulate solid-solution strengthening. The first one utilizes the materials properties calculated from ab initio calculations as the input to the solid-solution strengthening models developed in the framework of linear elasticity theory (e.g. [1–6]). This approach is very efficient, but the linear elasticity models used cannot properly describe dislocation cores. Consequently, the predictions can be qualitatively incorrect. For example, in the case of Al–Mg and Al–Li solid solutions, the strengthening capability of Li in Al is predicted to be higher than that of Mg, but the experimentally detected strengthening shows the opposite behavior (for details see Appendix A).

The second approach is to fully describe the interaction between the dislocation core and the solute atom(s) by the ab initio method. Simulations based on this approach should hence describe the solid-solution strengthening [7–10] and softening [11] very accurately. The approach is, however, time consuming, computationally demanding and thus not entirely suitable for rapidly predicting solute strengthening in model alloy systems, and large-scale systematic alloy screening.

In this study we aim at merging the advantages of the two approaches outlined above, and at developing a computationally efficient and quantitatively accurate approach to the prediction of solid-solution strengthening. In the first step, the dislocation core is described by the 2-D Peierls–Nabarro model [12,13]. In the second step, the pressure and displacement fields obtained from the 2-D Peierls–Nabarro model are used to capture the interaction between a solute and a straight dislocation. The third step is to homogenize this "dislocation–single solute" interaction effect into a net "dislocation–multiple solute" interaction form by using the solid-solution strengthening model recently developed by Leyson et al. [7–9] for calculating the critical resolved shear stress (CRSS) at 0 K and finite temperatures. This solid-solution strengthening model is a Labusch-type weak pinning model [14–16]. In principle, the third step could be alternatively replaced by a Friedel–Fleischer-type strong pinning model [17,18]. It has been observed, though, that for most cases, when the temperature is above 78 K and the solute concentration is above 0.01 at.%, the Labusch-type model becomes more appropriate compared to the Friedel–Fleischer-type model [19]. Thus, considering the Labusch-type model is likely to be suited for most engineering solid-solution alloys.

This paper is organized as follows: Section 2 outlines the theoretical methods employed in this study, including the solid-solution strengthening model developed by Leyson et al. [7–9], the 2-D Peierls–Nabarro model developed by Schoeck [12,13], and the corresponding ab initio

* Corresponding author. Tel.: +49 211 6792 330; fax: +49 211 6792 333; e-mail: d.ma@mpie.de

http://dx.doi.org/10.1016/j.actamat.2014.10.044
1359-6462/

calculations to obtain the necessary material properties to carry out the predictions; in Section 3.1, the dislocation–solute interactions in Al–Mg and Al–Li are to be shown; in Section 3.2, we present the predicted critical resolved shear stress vs. temperature curves of Al–Mg and Al–Li solid solutions compared with experiments; in Section 3.3, we employ a parametric study to show the dependence of the solid-solution strengthening capability on the strengthening parameters which are defined in Section 2.2.2; in Section 3.4, we compare the predictions by the parametric study described in Section 3.3 with the previous studies in which the dislocation–solute interactions are directly calculated by the ab initio method [7,8], and the experiments [62,63]; Section 4 summarizes our findings.

2. Methodology

In this section, we present the approach in a reverse manner, because the necessary input parameters are from the previous step(s). First we briefly describe the solid-solution strengthening model developed by Leyson et al. [7–9]; then the 2-D Peierls–Nabarro model used in this study, and how the dislocation–solute interaction energies are calculated from the 2-D Peierls–Nabarro model; finally we present the ab initio calculations used to obtain the necessary materials properties to carry out this approach.

2.1. Solid-solution strengthening model [7–9]

The solid-solution strengthening model developed by Leyson et al. [7–9] is related to the Labusch model for dense solute arrays [14–16]. This model describes the following process: in an infinite crystal of a pure metal, a single isolated dislocation is at its minimum energy, hence it assumes a straight form. In a solid solution with randomly distributed solute atoms, a straight dislocation should spontaneously bow-out, relaxing to its energetically favorable shape due to the local arrangement of the solutes. The final relaxed shape of the dislocation results from two competing processes. First, the binding energy (E_p) of the dislocation to the local region is decreased, while, second, the line energy (E_{el}) is increased due to the bow-out configuration. The bow-out shape is characterized by two parameters: the characteristic segment length (L_c) and the characteristic bow-out distance (ω_c), both of which can be determined by minimizing the total dislocation energy ($E_{tot}=E_p+E_{el}$). At 0 K, the critical resolved shear stress (CRSS) corresponds to the applied stress which is required to move a dislocation segment of characteristic length (L_c) over a characteristic bow-out distance of (ω_c). At finite temperature, the movement of the dislocation can be thermally activated. The details of the analytical derivation of this model can be found in Refs. [7–9].

To carry out this model, the dislocation–solute interaction energy is required. This interaction energy can be approximated by elastic models (e.g. [2,3]), or fully by ab initio calculations (e.g. [7–10]). In this study, the interaction energy is determined by using the 2-D Peierls–Nabarro model suggested by Schoeck [12,13].

It should be mentioned that the dislocation line tension has to be incorporated into this analysis for describing the bow-out of the dislocation. In the previous work of Leyson et al. [7,8], the dislocation line tension of Al was obtained from atomistic simulations (embedded atom method (EAM) potential). In this study, the dislocation line tension of Al is obtained from the isotropic linear elasticity [20], which is justified since Al has a relatively low elastic anisotropy with a Zener ratio of $A_Z \approx 1.3$. The line tension obtained from isotropic linear elasticity is 0.43 eV/Å for edge and 1.58 eV/Å for screw dislocations. The order of magnitude of these values is the same as those obtained from atomistic simulation, namely 0.25 eV/Å [7] or 0.47 eV/Å [8] for edge, and 1 eV/Å for screw dislocations [21]. The elastic constants used to determine the line tension are obtained by ab initio calculations in conjunction with Hershey's homogenization method [27] (see Section 2.3).

2.2. Dislocation–solute interaction by 2-D Peierls–Nabarro model

As described in the previous section, the solute position dependent dislocation–solute interaction energy is required to carry out the solid-solution strengthening model by Leyson et al. [7–9]. In this study, the interaction energy is obtained by inserting the misfit parameters into the pressure and displacement field obtained from the 2-D Peierls–Nabarro model. In this section, we first briefly describe the 2-D Peierls–Nabarro model developed by Schoeck [12,13], and then introduce the misfit parameters, i.e. volume and misfit parameters.

2.2.1. Equilibrium dislocation configuration using the 2-D Peierls–Nabarro model [12,13]

In the 2-D Peierls–Nabarro model developed by Schoeck [12,13], the equilibrium configuration of a straight dislocation is determined by minimizing the dislocation energy with respect to the adjustable geometrical parameters in the trial functions:

$$u_{\parallel} = \sum_i \left(\frac{Z_i}{\pi} \arctan\left(\frac{x + d_i}{\omega_i} \right) + \frac{Z_i}{2} \right)$$
$$u_{\perp} = \sum_i \left(\frac{Y_i}{\pi} \arctan\left(\frac{x + k_i}{v_i} \right) + \frac{Y_i}{2} \right) \quad (1)$$

where $u_{\parallel}$ and $u_{\perp}$ are the displacement profiles which are parallel and perpendicular to the total Burgers vector, respectively; Z_i and Y_i are the Burgers vectors of the fractional dislocations which are parallel and perpendicular to the total Burgers vector, respectively; d_i and k_i are positions of the fractional dislocations; ω_i and v_i are the width of the fractional dislocations. The trial functions serve to approximate the displacement profiles of the fractional dislocations. The dislocation energy comprising the elastic energy and the misfit energy can be calculated using the trial functions together with the knowledge of the elastic modulus and the γ-surface of the pure metal in consideration. The dislocation energy is minimized with respect to Z_i, Y_i, d_i, k_i, ω_i, and v_i, with one constraint that the sum of Burgers vectors of the fraction dislocations must be the same to the Burgers vector of the dislocation.

In this study, the equilibrium configuration of the straight dislocation in pure Al is determined by assuming two triplet partial dislocations as proposed in Ref. [12]:

$$u_{[110]} = \frac{Z_1}{\pi}\arctan\left(\frac{x+(d/2+i)}{\omega_1}\right) + \frac{Z_2}{\pi}\arctan\left(\frac{x+d/2}{\omega_1}\right) + \frac{Z_3}{\pi}\arctan\left(\frac{x+(d/2-i)}{\omega_1}\right) + \frac{Z_4}{\pi}\arctan\left(\frac{x-(d/2-i)}{\omega_1}\right) + \frac{Z_5}{\pi}\arctan\left(\frac{x-d/2}{\omega_1}\right) + \frac{Z_6}{\pi}\arctan\left(\frac{x-(d/2+i)}{\omega_1}\right) + \frac{b}{2}$$

$$u_{[1\bar{1}2]} = \frac{Y_1}{\pi}\arctan\left(\frac{x+(k/2+j)}{\omega_2}\right) + \frac{Y_2}{\pi}\arctan\left(\frac{x+k/2}{\omega_2}\right) + \frac{Y_3}{\pi}\arctan\left(\frac{x+(k/2-j)}{\omega_2}\right) + \frac{Y_4}{\pi}\arctan\left(\frac{x-(k/2-j)}{\omega_2}\right) + \frac{Y_5}{\pi}\arctan\left(\frac{x-k/2}{\omega_2}\right) + \frac{Y_6}{\pi}\arctan\left(\frac{x-(k/2+j)}{\omega_2}\right) \quad (2)$$

where

$$\sum_{i=1}^{3} Z_i = \sum_{i=4}^{6} Z_i = \frac{b}{2}, \quad \sum_{i=1}^{3} Y_i = -\sum_{i=4}^{6} Y_i = \frac{s\sqrt{3}b}{6}$$

where b is the Burgers vector of $\frac{1}{2}[110]$. In the above equation, if $s = 1$, the Burgers vectors of the triplet partial dislocations is exactly the same as the Schockley partial dislocations in a face-centered cubic (fcc) structure. In this study, we set s as an adjustable parameter, i.e. the total energy of the dislocation is minimized with respect to s, together with Z_n, Y_n ($n = 1,2,\ldots,6$), d, k, i, j, ω_1, and ω_2 in Eq. (2). It turned out that $s \approx 1.07$ and $s \approx 1.04$ for the edge and the screw, respectively. In order to reduce the number of the free parameters in Eq. (2), we follow the simplification in Ref. [12], namely set Z_2 and Y_2 to be free adjustable parameters, and the other Z_i and Y_i are dependent parameters:

$$Z_1 = Z_3 = Z_4 = Z_6, \quad Z_2 = Z_5$$
$$Y_1 = Y_3 = -Y_4 = -Y_6, \quad Y_2 = -Y_5$$

Instead of using the Rayleigh–Ritz method as employed in Ref. [12], the particle swarm optimization (PSO) algorithm [22][1] is used here for the dislocation energy minimization procedure. The optimized adjustable parameters in this study are in good agreement with the ones presented in Ref. [12]. According to the invariant misfit energy theorem [13], the misfit energy should be at the same value of $\mathbf{b}H\mathbf{b}$, where $\mathbf{b}$ is the Burgers vector; H is the symmetric Stroh tensor of the prelogarithmic energy factors in which the factor $1/4\pi$ is included for convenience [13]. The validity of the solution can be further checked by comparing the misfit energy obtained from the minimization procedure and $\mathbf{b}H\mathbf{b}$. The difference is 0.1% for edge and 0.6% for screw dislocation, which underlines the good quality of the solutions. To further assert the dislocation core description by using the 2-D Peierls–Nabarro model, the dislocation dissociations are determined and compared with the flexible-boundary DFT model (FB-DFT) and with experiments. The dislocation dissociations are determined by measuring the distance between the extrema in the dislocation density profiles[2] as shown in Fig. 1. The dissociation distance is 8.3 Å for the edge, and 5.2 Å for the screw. By using FB-DFT and the Nye tensor distribution given in Ref. [23], the dissociation distance in Al is determined to be 7.5 Å for the edge, and 5.0 Å for the screw. The dissociation distance of the edge determined by using a weak beam TEM observation is 8 Å [24] (the intensity profile can be found in Ref. [25]). Thus, the dislocation dissociations in Al are reasonably reproduced by using the 2-D Peierls–Nabarro model developed by Schoeck [12,13], which also gives certain confidence in the dislocation core description provided by the 2-D Peierls–Nabarro model.

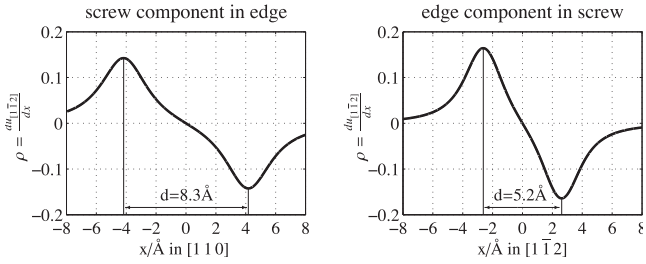

Fig. 1. The dislocation density distribution (ρ) of the screw component in the edge (left) and the edge component in the screw (right) by using the 2-D Peierls–Nabarro model. The dislocation dissociation distance is determined by measuring the distance between the extrema in the dislocation density profiles. The dissociation distance is 8.3 Å for the edge, and 5.2 Å for the screw. By using flexible boundary DFT (FB-DFT) and the Nye tensor distribution in Ref. [23], the dissociation distance is determined to be 7.5 Å for the edge, and 5.0 Å for the screw in Al. The dissociation distance of the edge determined by using a weak-beam TEM observation is 8 Å [24] (the intensity profile can be found in Ref. [25]). Thus, the dislocation dissociations in Al are reasonably reproduced by using the 2-D Peierls–Nabarro model developed by Schoeck [12,13].

Once the adjustable parameters in the trial functions (Eq. (2)) are determined, the pressure field of the dislocation and the displacement profile on the slip plane are extracted, and the misfit parameters are incorporated into the pressure field and the displacement profile to determine the dislocation–solute interaction energy. The misfit parameters are introduced in the next subsection by introducing two contributions to the dislocation–solute interaction energy: volume and slip interaction energy.

2.2.2. Dislocation–solute interaction

The dislocation–solute interaction energy is approximated by two contributions:

$$E_{\text{int}}(x,y) = E_{\text{volume}}(x,y) + E_{\text{slip}}(x,y) \quad (3)$$

where E_{volume} is the interaction energy due to volume misfit of the solute atom against the pressure field of the dislocation, and E_{slip} is the interaction energy due to the change of the γ-surface in the presence of the solute atoms proposed

[1] The general description of the algorithm is the following: a population (swarm) of possible solutions (particles) are moving around in the solution space guided by their individual best-known solutions and the best-known solution of the entire population; newly discovered best solutions will then guide the movement of the particles; this process is repeated, and gradually the particles will converge to the real solution [22].

[2] The dislocation density profile is determined by: $\rho = \frac{du}{dx}$ [12,13,26].

Table 1. Correspondence of the symbols between Eqs. (4) and (2).

Edge		Screw	
Eq. (4)	Eq. (2)	Eq. (4)	Eq. (2)
b_{e_1}	Z_1	b_{e_1}	Y_1
b_{e_2}	Z_2	b_{e_2}	Y_2
b_{e_3}	Z_3	b_{e_3}	Y_3
b_{e_4}	Z_4	b_{e_4}	Y_4
b_{e_5}	Z_5	b_{e_5}	Y_5
b_{e_6}	Z_6	b_{e_6}	Y_6
d_{e_1}	$-d/2-i$	d_{e_1}	$-k/2-j$
d_{e_2}	$-d/2$	d_{e_2}	$-k/2$
d_{e_3}	$-d/2+i$	d_{e_3}	$-k/2+j$
d_{e_4}	$d/2-i$	d_{e_4}	$k/2-j$
d_{e_5}	$d/2$	d_{e_5}	$k/2$
d_{e_6}	$d/2+i$	d_{e_6}	$k/2+j$
ω_e	ω_1	ω_e	ω_2

by Yasi et al. [10]. E_{slip} is conceptually the same term as the di-elastic energy proposed by Fleischer [2,3]. Since the shear close to the dislocation core is more adequately described as the shear between interatomic layers, the γ-surface is a more pertinent material property than the shear modulus to characterize the di-elastic effect.

Volumetric misfit interaction energy: (E_{volume}) After the equilibrium configuration of the dislocation in the pure metal is obtained, the optimized Burgers vectors and the positions of the edge fractional dislocations can be used to calculate the pressure field produced by the dislocation [26]:

$$p(x_n,y_m)=-\frac{G(1+\nu)}{3\pi(1-\nu)}\sum_{i=1}^{i=N}b_{e_i}\times\frac{y_m+\text{sign}(y_m)\omega_e}{(x_n-d_{e_i})^2+(y_m+\text{sign}(y_m)\omega_e)^2} \tag{4}$$

where G and ν are the homogenized[3] (polycrystal averaged) shear modulus and Poisson's ratio of the pure metal; N is the number of the edge fractional dislocations assumed in the 2-D Peierls–Nabarro model, which is 6 in this study, because two triplet partial dislocations are assumed; b_{e_i} and d_{e_i} are the Burgers vectors of the edge fractional dislocations and the corresponding positions, respectively; ω_e is the width of the edge fractional dislocation. The correspondence of the symbols between Eqs. (4) and (2) is listed in Table 1. The pressure field is calculated by isotropic elasticity which is an acceptable approximation for Al, because the Zener's ratio of Al is close to 1 (≈ 1.3). For other systems, especially the ones being highly elastically anisotropic, applying anisotropic elasticity is mandatory. At the end of this section, we shall discuss further about applying anisotropic elasticity treatment to the dislocation in the proposed approach in this study.

In addition, instead of using a continuum field, a discrete lattice field is used. In order to create a dislocation, the crystal is cut along the plane at $y=0$ (y-axis is perpendicular to the slip plane, z-axis is parallel to the dislocation line). Then the upper crystal is displaced by $1/2\times u_x(x)$ and the lower crystal by $-1/2\times u_x(x)$, where $u_x(x)$ is the displacement along the x axis as obtained from the 2-D Peierls–Nabarro model. The resulting dislocation structure is shown in Fig. 2. Since the pressure field is independent of z (see Eq. (4)), technically there is no need to consider any displacement along z. Thus, the positions of the atoms pertaining to the dislocation core are determined in an approximated but very reasonable way, and the stress singularity problem is avoided naturally. Accordingly, in evaluating the characteristic bow-out distance, ω_c, of a dislocation in a randomly distributed solid solution, only discrete values are taken, namely nb for the edge dislocation and $n\sqrt{3}b$ for the screw dislocation, where n is an integer number and b is the Burgers vector $\frac{1}{2}[110]$. With the pressure field, E_{volume} can next be calculated by:

$$E_{\text{volume}}(x_n,y_m)=-p(x_n,y_m)\times\Delta V \tag{5}$$

where ΔV is the extra volume introduced by the solute atom in the matrix. In this study, we define the volume misfit parameter in terms of the lattice parameter and not in terms of the extra volume:

$$\Delta V=\frac{3a_0^3}{4}\times\varepsilon_b \tag{6}$$

$$\varepsilon_b=\left(\frac{1}{a}\times\frac{da}{dc}\right)_{c=0} \tag{7}$$

where c is the atomic fraction of the solute element; a_0 is the lattice parameter of pure Al; and ε_b is the volume misfit parameter.[4] In this study, the lattice parameters in Eqs. (6) and (7) are determined by using the ab initio method (see Section 2.3).

The volume misfit parameter in Eq. (6) was originally proposed by Cottrell [28]. It is derived only from the geometrical quantities, such as the lattice parameter or the atomic volume. There is another parameter to capture the volume misfit proposed by Eshelby [29] which is determined by studying the stress–strain response of a volume containing a point defect under an external strain–stress field. The volume misfit parameter proposed by Eshelby is referred as the "strength of a point defect" or the "elastic dipole". Essentially, Eshelby's proposal not only takes the extra volume of the solute into account, but also the change in the chemical bonds. Thus, the volume misfit parameter proposed by Eshelby is a more appropriate parameter to evaluate E_{volume}. On the other hand, by using atomistic simulation, it has been shown that in fcc substitutional solid solutions, the volume misfit parameter proposed by Cottrell can be used to accurately predict E_{volume} [30], mostly because the dilatation center caused by a substitutional atom in fcc is spherical [31]. In body-centered cubic (bcc) interstitial solid solutions, e.g. C in α-Fe [31,32], however, one has instead to use the volume misfit parameter proposed by Eshelby, because the dilatation center caused by an interstitial atom in bcc is non-spherical.

At the end of this section we should briefly reflect on the application of anisotropic elasticity in the context of the proposed approach. In this study, we use Al binary solid-solution alloys as a representative class of metallic materials. Since the Al matrix is nearly elastically isotropic

[3] In this study, the homogenized values for G and ν are obtained by using Hershey's homogenization method [27] in conjunction with the elastic stiffness tensor obtained from the ab initio calculations (see Section 2.3).

[4] Let V and a be the volume of an atom and the lattice parameter of a fcc unit cell, and in fcc there are 4 atoms in a unit cell, then: $V=\frac{1}{4}a^3\Rightarrow\frac{dV}{dc}=\frac{1}{4}\times3a^2\frac{da}{dc}\Rightarrow\frac{dV}{dc}=\frac{1}{4}\times3a^3\frac{1}{a}\frac{da}{dc}\Rightarrow\left(\frac{dV}{dc}\right)_{c=0}=\frac{1}{4}\times3\left(a^3\frac{1}{a}\frac{da}{dc}\right)_{c=0}\Rightarrow\Delta V=\frac{3}{4}a_0^3\varepsilon_b$, where $\varepsilon_b=\left(\frac{1}{a}\frac{da}{dc}\right)_{c=0}$ is the volume misfit parameter.

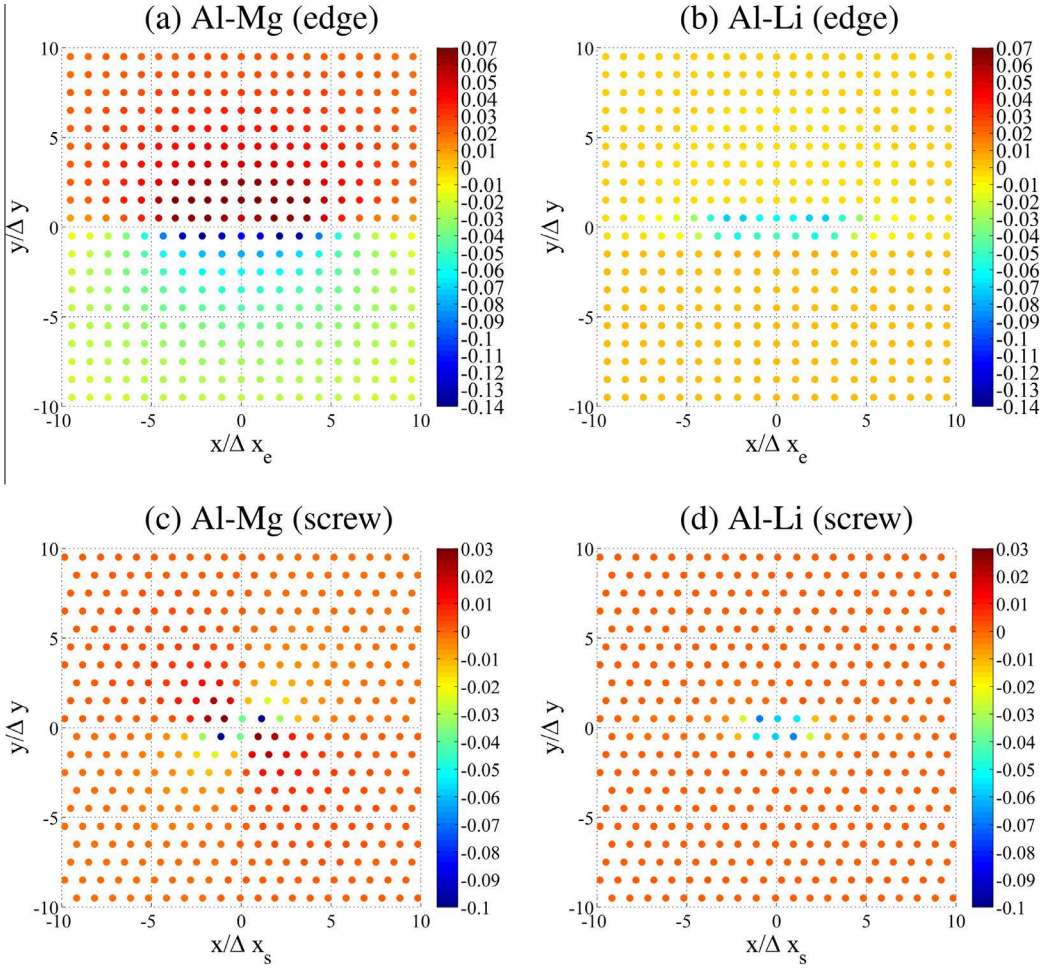

Fig. 2. Position-dependent dislocation–solute interaction energy in Al–Mg (a and c) and Al–Li (b and d). $\Delta y = a_{Al}\sqrt{3}/3$, $\Delta x_e = b/2$, and $\Delta x_s = b\sqrt{3}/2$, where a_{Al} and b is the lattice parameter of pure Al and the Burgers vector on $[\bar{1}\,1\,0](1\,1\,1)$ slip system, respectively. Note: the color scales are different for the edge and screw dislocation. (For interpretation of the references to color in this figure legend, the reader is referred to the web version of this article.)

($A_Z = 1.3$), isotropic elasticity is a reasonable approximation of the dislocation self-stress and distortion fields. In the proposed approach, linear elasticity theory enters with respect to three aspects: (i) the dislocation line tension (see Section 2.1); (ii) the prelogarithmic energy factor for the elastic energy of the dislocation when applying the 2-D Peierls–Nabarro model (see [12,13]); (iii) the stress field created by the dislocation which is required for obtaining the pressure field as described in this section. All three aspects are not limited to the use of elastic isotropy of the elemental matrix materials, but all properties can be calculated analytically or numerically also for the case of linear elastic anisotropic dislocation fields [26,33].

Slip misfit interaction energy: (E_{slip}) The slip interaction energy is defined as:

$$E_{\text{slip}}(x_n, y_m) = A_a \times (\gamma_{\text{Al–X}}(\mathbf{u}(x_n, y_m)) - \gamma_{\text{Al}}(\mathbf{u}(x_n, y_m))) \tag{8}$$

where $\mathbf{u}$ is the shear displacement on the slip plane; A_a is the area occupied by one atom on the slip plane; and $\gamma_{\text{Al–X}}$ and γ_{Al} are the γ-surfaces of Al–X solid solution and pure Al on the slip plane, respectively. In this study, two approximations were made, which have been proven to be reasonable [7,10]:

1. Except the shear between the atomic layers immediately above and below the slip plane, the shear between two adjacent atomic layers is ignored. Thus, the predominant slip interaction energy comes from the atomic planes immediately above and below the slip plane.
2. The γ-surface of the solid solution ($\gamma_{\text{Al–X}}$) is approximated by scaling the γ-surface of pure Al (γ_{Al}) on the slip plane by a factor of $\frac{\gamma_{\text{Al–X,I2}}}{\gamma_{\text{Al,I2}}}$, where I2 refers to the intrinsic stacking fault.

With these two approximations, Eq. (8) can be written:

$$E_{\text{slip}}(x_n, y_{\pm 1}) = A_a \times \gamma_{\text{Al}}(\mathbf{u}(x_n, y_{\pm 1})) \times \varepsilon_s \tag{9}$$

$$y_{\pm 1} = \pm\frac{1}{2} \times \frac{\sqrt{3}}{3} \times a_0$$

$$\varepsilon_s = \frac{1}{\gamma_{\text{Al,I2}}} \times \frac{d\gamma_{\text{Al–X,I2}}}{dc_{\text{sf}}}$$

where c_{sf} is the atomic concentration of the solute atoms on the stacking fault; ε_s is the slip misfit parameter proposed by Yasi et al. [10].

2.3. Ab initio calculations

According to Sections 2.1 and 2.2, the necessary materials properties for predicting solid-solution strengthening of Mg and Li in Al are the following: the lattice parameter, the polycrystalline shear modulus and the Poisson's ratio, and the γ-surface of pure Al; and the compositional dependence of the lattice parameters and the intrinsic stacking fault energy of Al–X. All these parameters are here calculated by ab initio methods.

The ab initio calculations were performed based on density functional theory (DFT) as implemented in the Vienna Ab initio Simulation Package (VASP) [34,35]. PBE [36] was selected as the exchange–correlation functional. The PAW [37] method was used to describe the elements with their respective electronic configurations of the core electrons: Al ($3s^2 3p^1$), Mg ($2p^6 3s^2$) and Li ($1s^1 2s^1 2p^1$), where the valence electrons are listed in brackets, and for the PAW potential of Li, the semi-core s states are treated as valence states. The cut-off energy was 420 eV in all cases. The equivalent k-point sampling was $24\times24\times24$ using the Monkhorst–Pack method [38]. The Fermi surface is smeared out by using the Methfessel–Paxton smearing scheme [39] taking $\sigma = 0.4$ eV. The calculated lattice parameter and the bulk modulus are converged within 0.002 Å and 0.1 GPa when using the above simulation setup.

The lattice parameter (a_0) and the bulk modulus (B, compressive modulus) were calculated by using the Birch–Murnaghan fit [40,41]. Two elastic constants, $C_{11} - C_{12}$ and C_{44}, were calculated by using the energy-strain approach (e.g. [42]). The individual C_{11} and C_{12} are derived from the calculated bulk modulus ($B = C_{11} + 2C_{12}$) and $C_{11} - C_{12}$. The calculated lattice parameter and the elastic constants of pure Al are $a_0 = 4.040$ Å, $C_{11} = 112.2$ GPa, $C_{12} = 60.1$ GPa and $C_{44} = 33.6$ GPa, being in good agreement with corresponding values obtained from experiments ($a_0 = 4.032$ Å [43] $C_{11} = 114.43$ GPa, $C_{12} = 61.92$ GPa and $C_{44} = 31.62$ GPa [44]. After C_{11}, C_{12} and C_{44} are obtained, Hershey's homogenization method [27] is used to homogenize the calculated elastic constants to obtain the polycrystalline shear modulus and Poisson's ratio for the case of a material with random crystallographic texture. It should be noted that when calculating the elastic constants of soft elements, such as Al, the magnitude of the elastic strain energy can be so small that it is comparable to the computational errors of the ab initio calculations themselves. On the other hand, when larger strains are applied, the elastic response is beyond second-order elasticity and the second-order polynomial fitting of computed energies is not sufficient. Therefore, we performed convergence tests related to the post-processing of computed strain energies and it was found that when the magnitude of the applied strain is higher than 6% and fourth-order polynomial functions are used for fitting, the $C_{11} - C_{12}$ and C_{44} elastic constants become independent of the magnitude of the applied strain.

Table 2. Calculated misfit parameters, ε_b and ε_s, of Al–Mg and Al–Li solid solutions.

	ε_b	ε_s
Al–Mg	0.104	−0.38
Al–Li	−0.007	−0.68

To calculate the compositional lattice parameter, two supercells with five compositions were used, namely $Al_{107}X_1$, $Al_{105}X_3$, $Al_{31}X_1$, $Al_{104}X_4$ and $Al_{30}X_2$. The solute atoms in the supercell are ordered in such a way that the cubic symmetry of the supercell is still maintained. The calculated compositional dependences of the lattice parameter of Al–Mg and Al–Li are 0.42016 Å/at. and −0.02828 Å/at., respectively, in very good agreement with the experiments: 0.44844 Å/at.[45] and −0.02828 Å/at. [46].

The γ-surface of pure Al calculated by Wu et al. [47] is taken as the input into the 2-D Peierls–Nabarro model. The compositional intrinsic stacking fault energy is calculated by using the slab model (e.g. [48] with 12 layers of (1 1 1) planes, and the solute atom concentration on the stacking fault is 25%.

3. Results and discussion

3.1. Dislocation–solute interaction energy in Al–Mg and Al–Li

Using the strengthening parameters of Mg and Li in Al solid solution listed in Table 2 from ab initio calculations, E_{volume} and E_{slip} can be obtained according to Eqs. (5) and (9). The sum of E_{volume} and E_{slip}, namely the total dislocation–solute interaction energy, is shown for Al–Mg and Al–Li in Fig. 2.

The dislocation–solute interaction energy in Al–Mg is positive in the compressed side and negative in the expanded side, because Mg introduces large and positive extra volume, even though its slip misfit parameter is negative. Li, on the other hand, has negative but negligible extra volume in Al, and a relatively large negative slip misfit parameter. Therefore, the dislocation–solute interaction energy in Al–Li could be negative even in the expanded side. Al–Li represents an extreme case that only the slip misfit contributes to the solid-solution strengthening.

The position-dependent dislocation–solute interaction energies shown in Fig. 2 are used as input to the solid-solution strengthening model developed by Leyson et al. [7–9]. The dislocation–solute interaction energies are used to determine the characteristic segment length (L_c) and the characteristic bow-out distance (ω_c) of a dislocation in a solid solution with randomly distributed solute atoms. In turn, L_c and ω_c are used to determine the energy barrier (ΔE_b) against the dislocation motion in a randomly distributed solid solution, and the shear stress (τ_0) to overcome this energy barrier at 0 K. At finite temperature, overcoming ΔE_b can be aided by the thermal activation. The detail of the model is referred to Refs. [7–9].

3.2. Comparison of τ_0 vs. temperature curves of Al–Mg and Al–Li solid solutions between theory and experiments

By using the dislocation–solute interaction energy in Fig. 2 as input to the solid-solution strengthening model [7–9], τ_0 (i.e. the critical resolved shear stress (CRSS)) of Al–Mg and Al–Li at finite temperatures can be predicted. Figs. 3 and 4 show the comparison between the theoretically and experimentally determined τ_0 vs. temperature for Al–Mg (Fig. 3) and Al–Li (Fig. 4). The predictions and experiments reveal a better match in the intermediate temperature regime than at elevated temperatures.

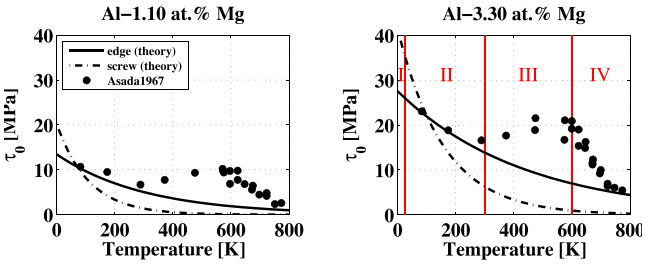

Fig. 3. The comparison between theoretically and experimentally determined τ_0 (CRSS, critical resolved shear stress) vs. temperature in Al–Mg systems. Experimental values are from Ref. [49]. On the right, four temperature regimes are indicated as defined in Ref. [52]. Note that the divisions of the temperature regimes are approximated. A rigorous identification of the boundaries should be made with the help of the respective stress–strain-rate sensitivity vs. temperature curves [52]. It should be mentioned that the boundary between regime I and II (~25 K) is taken from the work by Podkuyko and Pustovalov [57] in which tensile tests were conducted on Al–Mg single crystals from 1.6 to 300 K.

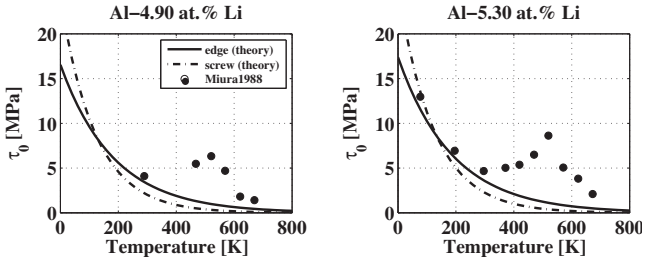

Fig. 4. The comparison between theoretical and experimental determined τ_0 (CRSS, critical resolved shear stress) vs. temperature in Al–Li systems. Experimental values are from Ref. [50].

According to Caillard and Martin [52], the τ_0 vs. temperature curve can be divided into four temperature regimes (temperature ranges are in ascending order): (I) underdamped regime, i.e. the dislocations are able to pass through an array of solute atoms with the help of inertia, because the phonon friction is very low and the velocities of the dislocations can be very high [53,54]. (II) Overdamped regime, i.e. the phonon friction becomes high, and dislocations can pass the solutes with the aid of thermal activation. (III) Stress instability regime and Portevin–LeChâtelier (PLC) effect regime. (IV) Dislocation motion is controlled by the solute atmosphere, due to the high mobility of the solute atoms. These temperature regimes are indicated on the right-hand side of Fig. 3. Note that the transitions between these adjacent temperature regimes are only approximated. A more rigorous identification of the boundaries should be made with the help of the respective stress–strain-rate sensitivity vs. temperature curves [52]. In Figs. 3 and 4, the theoretical predication starts to deviate from the experimental observations at that temperature where regime III begins, i.e. where the PLC effect starts to operate. Thus, from this temperature on, it is more appropriate to employ other models, such as the cross-core model proposed by Curtin and co-workers [56], to simulate the PLC effect.

In regime II, a plateau regime (τ_0 is insensitive to the temperature) can be observed in some other alloy systems, such as Cu-based (e.g. [52]) and Mg-based solid solutions (basal slip, e.g. [55]). This effect cannot, however, be observed in Figs. 3 and 4. A plausible explanation for this discrepancy is the dislocation dissociation distance [9]. In Cu and Mg (basal slip), the dislocation dissociation distance is much larger than for Al, due to their much lower stacking fault energies compared to that of Al. By using the dislocation–solute interaction energy calculated by the ab initio method and the same solid-solution strengthening model, it is observed that in basal slip of Mg–Al, two characteristic bow-out distances (ω_c) can be found. Moving the dislocation by the small ω_c decorrelates the solute fluctuations within the partial dislocations, and moving by the large one decorrelates with the solute atoms far away from the dislocation core. These two characteristic bow-out distances correspond to two dislocation configurations. Each configuration is associated with a specific energy barrier against dislocation motion. Below the plateau regime, the solid-solution strengthening effect is governed by the configuration with a low energy barrier. In the plateau regime, the configuration with a high energy barrier prevails over the other configuration with a low energy barrier. Due to the high energy barrier, τ_0 appears to be insensitive to the temperature in the plateau regime. Since the dislocation dissociation in Al is rather small compared with that in Mg (basal slip), only one value of ω_c, i.e. only one dislocation configuration, can be found. Thus, the plateau regime can be hardly observed on the τ_0 vs. temperature curves in Figs. 3 and 4.

In Al–Mg and Al–Li (Figs. 3 and 4), the theoretically predicted τ_0 of the screw dislocation is higher than that of the edge dislocation at low temperature, e.g. $<\sim$70–80 K. It is usually believed that the interaction between the dislocation and the solute atoms is stronger for the edge than for the screw dislocation. This is indeed true for the energy barrier (ΔE_b) (see Table 5). ΔE_b of the edge dislocation is roughly 2.7 and 1.5 times that of the screw dislocation in Al–Mg and Al–Li, respectively. On the other hand, τ_0 is proportional to $\Delta E_b/\left(\omega_c^{5/3}\Gamma^{2/3}\right)$ [7–9], where ω_c of the screw dislocation is ~0.29 and ~0.43 of the edge dislocation, and the line tension (Γ) of the screw dislocation is ~3.7 times the value of the edge dislocation. Accordingly, at 0 K, τ_0 of the screw dislocation is higher than of the edge by $\sim 21\%/c^{2/3}$ and $\sim 12\%/c^{2/3}$ in Al–Mg and Al–Li solid solutions, where c is the atomic concentration. At finite temperature, since ΔE_b of the screw dislocation is lower than that of the edge dislocation, the motion of the screw dislocation can be more thermally activated than the that of the edge dislocation. Therefore, when the temperature is higher than ~70–80 K, τ_0 of the edge is larger than that of the screw.

Fig. 5 shows theoretically predicted and experimentally measured values of τ_0 vs. the solute content (here at.% Mg) at 290 K. The linear dependence of τ_0 on the concentration is reproduced. Unlike the observations in other fcc binary systems, such as Cu and Au binary systems, where $c^{2/3}$ dependence is even observed in the plateau regime [58,59]. The solid-solution strengthening model used in this study is very sensitive to the strain rate when compared with the experiments, because in the experiments, τ_0 varies within the range of ~1 MPa, if the strain rate changes from 1.5×10^{-5}/s to 2.5×10^{-2}/s, but the theoretical prediction varies even within 2–4 MPa. It should be noted that τ_0 of pure Al is not negligible in Fig. 5. If one subtracts from the experimentally determined τ_0 of the Al–Mg solid solutions the τ_0 of pure Al, a better agreement should be achieved.

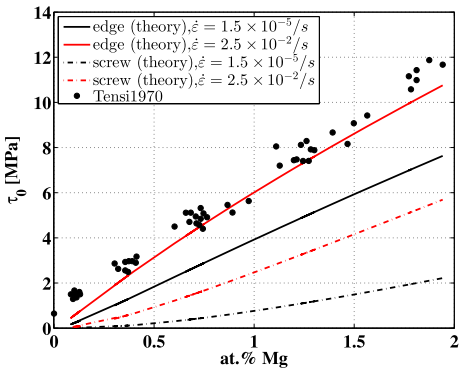

Fig. 5. The comparison between theoretically and experimentally determined τ_0 (CRSS) vs. at.% Mg at 290 K in Al–Mg systems. Experimental values are from Ref. [51]. In the original experiments, the shear rate ($\dot{\gamma}$) is varied between 3×10^{-5}/s and 5×10^{-2}/s. According to the extended Schimd law, $\left(\frac{d\gamma}{dt}\right)_{t=0} \cos\kappa_0 \sin\lambda_0 = \left(\frac{d\varepsilon}{dt}\right)_{t=0}$, where κ_0 and λ_0 is the original angle of the loading axis with respect to the slip direction and the slip plane normal, respectively. In Ref. [51], κ_0 and λ_0 are both $\pi/4$, which gives $\dot{\varepsilon} = 1/2\dot{\gamma}$.

3.3. Creating guideline maps of misfit parameters against τ_0 at 0 K and ΔE_b for Al solid solutions

The separation of the different energy contributions (E_{volume} and E_{slip}) to the dislocation–solute interaction allows a systematic study in which the misfit parameters (ε_b and ε_s) are parametrized to calculate the corresponding τ_0 at 0 K and ΔE_b. In this way, the dependences of the τ_0 at 0 K and ΔE_b on these two misfit parameters can be established. Those dependences can be considered to be guideline maps where τ_0 at 0 K and ΔE_b of any Al solid solution can be found by positioning its corresponding ε_b and ε_s on the guideline maps. In turn, one can use the knowledge of τ_0 at 0 K and ΔE_b to predict τ_0 at finite temperatures.

The characteristic bow-out length (ω_c) is firstly determined for each pair of the parameters ε_b and ε_s shown in Fig. 6. Within the investigated ranges of ε_b and ε_s, only three values for ω_c are found for the edge and two values for the screw dislocation, respectively (see Fig. 6).

Fig. 7 shows the energy barrier (ΔE_b) and τ_0 at 0 K of the screw and edge dislocations on the dependence of ε_b and ε_s. The energy barrier, ΔE_b for the edge dislocation is in general twice that observed for the screw dislocation. τ_0 of the screw dislocation at 0 K is larger than that of the edge dislocation. As already discussed in Section 3.2, this is mainly because the characteristic bow-out distance (ω_c) of the screw dislocations is shorter than that of the edge dislocations (see Fig. 6). Both ΔE_b and τ_0 at 0 K strongly depend on ε_b, even for the screw dislocation. This is because the dissociation of the dislocation is considered in this study, and the edge components of the dissociated screw dislocation can still produce a pressure field.

In the solid-solution strengthening model [7–9], the binding energy (ΔE_p) of the dislocation to a local region is captured by the standard deviation of the energy difference when a dislocation segment moves over a distance of ω. We assume that $\Delta E_p \sim \left(c_1\varepsilon_b^2 + c_2\varepsilon_s^2 + c_3\varepsilon_b\varepsilon_s\right)^{\frac{1}{2}}$, where c_i ($i = 1,2,3$) are constants. On the other hand, $\Delta E_b \sim \Delta E_p^{\frac{2}{3}}$ and $\tau_{0(\text{T}=0\,\text{K})} \sim \Delta E_p^{\frac{4}{3}}$ [7–9]. Thus, Fig. 7 can be approximated by the following fitting functions:

$$\Delta E_b/c^{\frac{1}{3}} = \left(\left(a_1 \times \varepsilon_b^2 + a_2 \times \varepsilon_s^2 + a_3 \times \varepsilon_b \times \varepsilon_s\right)^{\frac{1}{2}}\right)^{\frac{2}{3}} \text{eV} \tag{10}$$

$$\tau_{0(\text{T}=0\,\text{K})}/c^{\frac{2}{3}} = \left(\left(b_1 \times \varepsilon_b^2 + b_2 \times \varepsilon_s^2 + b_3 \times \varepsilon_b \times \varepsilon_s\right)^{\frac{1}{2}}\right)^{\frac{4}{3}} \text{MPa} \tag{11}$$

where a_i and b_i ($i = 1,2,3$) are fitting parameters. The cross-term implies that the misfits do not independently contribute to the strengthening. Depending on the sign of the misfit parameters, the dislocation–solute interaction can in principle become locally stronger or weaker [10]. The fitted parameters are listed in Table 3.

Table 3 indicates that in Al solid solutions, the solid-solution strengthening effect mostly depends on ε_b, and ε_s only plays a minor role. Let us first roughly estimate the overall error, if ε_s in Eqs. (10) and (11) is ignored. The coefficients before ε_b are in general two orders of magnitude larger than those before ε_s and the cross-term. Usually the range of ε_s is one order of magnitude larger

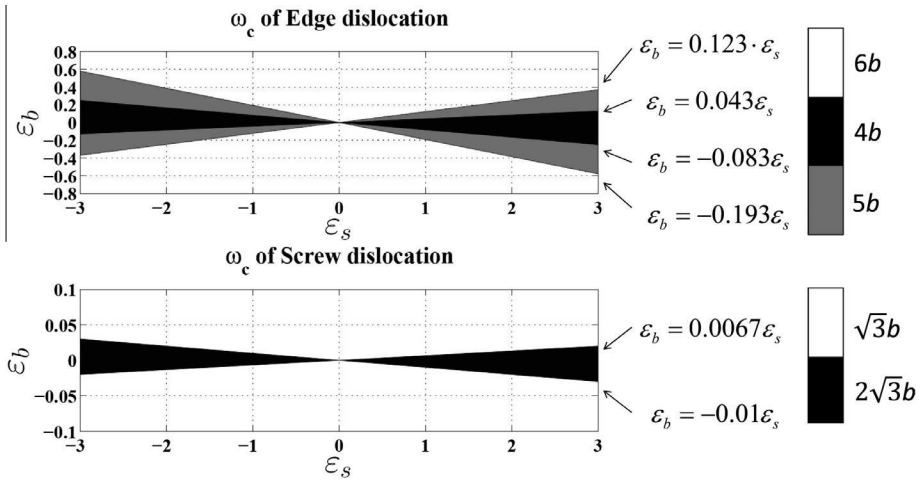

Fig. 6. The characteristic bow-out distance, ω_c, vs. ε_b (volume misfit parameter) and ε_s (slip misfit parameter). Three ω_cs are found for the edge dislocation: 6*b* (white region), 5*b* (gray region) and 4*b* (black region). Two ω_cs are found for the screw dislocation: $\sqrt{3}b$ (white region) and $2\sqrt{3}b$ (black region). The equations on the right-hand side bound these regions.

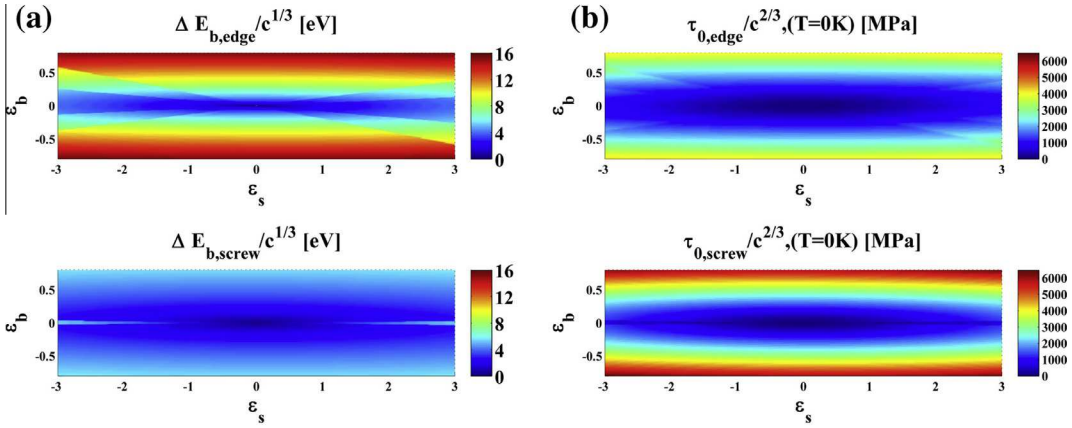

Fig. 7. Guideline maps of (a) $\Delta E_b/c^{1/3}$ and (b) $\tau_{0(T=0\,K)}/c^{2/3}$ vs. the misfit parameters, ε_b (volume misfit parameter) and ε_s (slip misfit parameter).

Table 3. The fitting parameters in Eqs. (10) and (11). The goodness of fit: SSE⟶0 and R^2⟶1.

	ω_c	$a_1 \times 10^{-3}$	$a_2 \times 10^{-1}$	$a_3 \times 10^{-1}$
Edge	$4b$	1.51	0.68	0.04
	$5b$	3.18	1.23	1.04
	$6b$	5.60	1.89	2.48
Screw	$\sqrt{3}b$	0.26	0.19	0.16
	$2\sqrt{3}b$	1.08	1.54	1.04
	ω_c	$b_1 \times 10^{-5}$	$b_2 \times 10^{-3}$	$b_3 \times 10^{-3}$
Edge	$4b$	6.81	3.04	0.18
	$5b$	5.52	2.04	1.71
	$6b$	4.07	1.38	1.80
Screw	$\sqrt{3}b$	7.16	5.31	4.53
	$2\sqrt{3}b$	1.32	1.89	1.27

than that of ε_b [60]. Thus, ignoring ε_s overall gives an error of the order of 0.1. Fig. 8 shows the errors, if ε_s is ignored in Eqs. (10) and (11), assuming ω_c is $6b$ for the edge and $\sqrt{3}b$ for the screw dislocation. As anticipated in Fig. 8, only if the magnitude of ε_s is small, will the error also be small. It is also interesting to insert the ε_b and ε_s of the solute elements in Al into Fig. 8 to see the consequence of ignoring Eqs. (10) and (11) in practice. A number of ε_b and ε_s of solute elements in Al calculated by the ab initio method [60] are plotted as black open circles in Fig. 8. Some of solute elements fall into the area where ignoring ε_s might introduce substantial errors (larger than 20%).

With the knowledge of τ_0 at 0 K and ΔE_b in Fig. 7, τ_0 at finite temperatures can be obtained by using the thermal activation models presented in Refs. [20,8,9]. Fig. 9 shows the predicted τ_0 at 100–300 K with 0.1 at.% concentration.

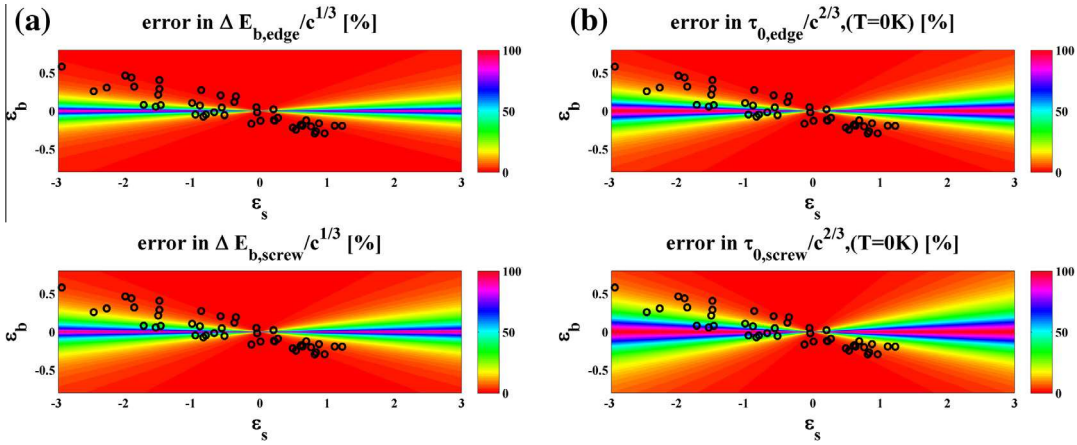

Fig. 8. Contour plots of the errors in (a) $\Delta E_b/c^{1/3}$ (b) $\tau_{0(T=0\,K)}/c^{2/3}$ vs. the misfit parameters, ε_b (volume misfit parameter) and ε_s (slip misfit parameter), if one ignores ε_s in Eqs. (10) and (11). It is assumed that ω_c is $6b$ for edge and $\sqrt{3}b$ for the screw dislocation. A number of ε_b and ε_s of the solute elements in Al are plotted as black open circles, and these data are from Ref. [60].

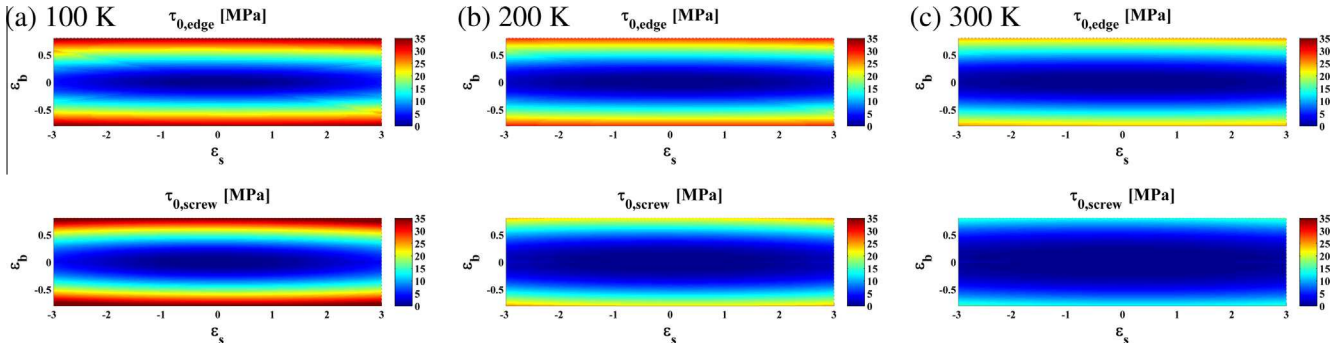

Fig. 9. τ_0 at $c = 0.1$ at.% at (a) 100 K (b) 200 K and (c) 300 K vs. the misfit parameters, ε_b and ε_s. The strain rate is assumed to be $\dot{\varepsilon} = 1 \times 10^{-3}$.

Since ΔE_b of the screw dislocation is roughly half that of the edge dislocation, the movement of the screw dislocation can be more easily thermally activated. At 100 K, τ_0 of the edge and the screw are comparable (also shown in Figs. 3 and 4). But above 100 K, τ_0 of the edge is much larger than that of the screw. Another observation is that as the temperature rises, τ_0 becomes less and less dependent on ε_s, and this particularly applies when ε_b is small. This can be better seen in Fig. 10. In the thermal activation model applied in this study (see Refs. [7–9,20] for details), the rate of decrease of τ_0 upon increasing temperature becomes slow as the temperature increases, and above a certain temperature the rate of decrease of τ_0 becomes negligible (see Eq. (28) in Ref. [8]). And this certain temperature is low when ΔE_b is low. Therefore, as the temperature rises, the τ_0 corresponding to a higher ΔE_b becomes similar to another τ_0 corresponding to a lower ΔE_b. This can be seen from Fig. 10: each curve corresponding to a specific ε_b becomes flatter and flatter, as the temperature increases, meaning that the difference in ΔE_b introduced by the variation of ε_s can be leveled off by increasing the temperature up to, for example, 300 K.

3.4. Prediction by the guideline maps and comparison with previous studies

In this section, we use the guideline maps obtained in the last section to predict the solid-solution strengthening effect of other elements in Al. We chose Cu, Si, Cr, Mn and Fe. The misfit parameters, ε_b and ε_s, of these elements in Al were calculated by using the ab initio method (see Section 2.3). It should be mentioned that the calculations were conducted without considering spin polarization, even in case of Cr, Mn and Fe. It has been shown that in Fe–Al solid solutions, the magnetic moment decreases down to 10% of the magnetic moment of pure bcc Fe, when Al is at 50 at.% [61]. Therefore, we expect that the influence of magnetism of these solutes is absent or very weak for the current cases assuming low solute concentrations in Al alloys. We first compare the results in this study with previous studies [7,8] in which very accurate dislocation–solute interactions were calculated by using FB-DFT, and then with experiments.

Table 4 lists the characteristic bow-out distance (ω_c) in the context of the Labusch model determined in this study compared with those in previous studies [7,8,21]. In this study, the dislocation partial dissociation is 8.3 Å (see Fig. 1) for the edge dislocation. ω_c of the edge dislocation is about 1.4–2 times the value of the dislocation dissociation. In Refs. [7,8], ω_c of the edge dislocation is 1.5 times as large as the dislocation dissociation. ω_c of the screw is mostly close to 5 Å which is the dislocation partial dissociation in this study (5.2 Å) (see Fig. 1). ω_c of the screw dislocation is usually smaller than that of the edge dislocation, which is also observed in Ref. [21] where the EAM potential was used. This can be explained by the fact that the

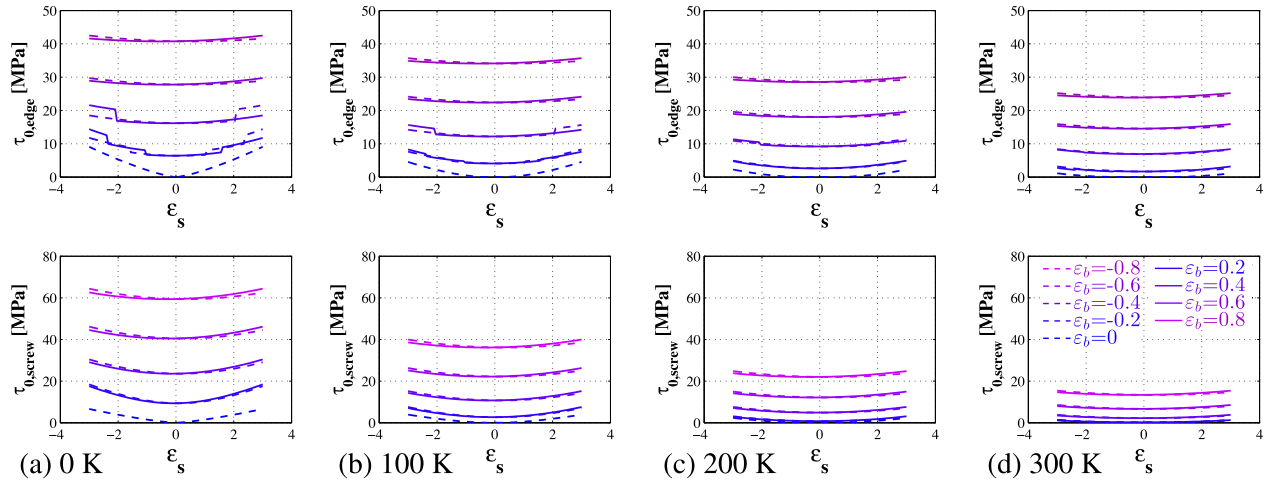

Fig. 10. τ_0 at $c = 0.1$ at.% at (a) 0 K (b) 100 K (c) 200 K and (d) 300 K vs. ε_s. The strain rate is assumed to be $\dot{\varepsilon} = 1 \times 10^{-3}$.

Table 4. The characteristic bow-out distance (ω_c in Å) in the context of Labusch model determined by using different dislocation–solute interaction descriptions: in Ref. [8] the dislocation–solute interaction is determined by using direct ab initio calculation; in Ref. [21], the EAM potential is used. It should be noted that, unlike in Ref. [8], in this study, ω_c only takes a discrete distance along the corresponding slip direction, i.e. for the edge, $6b = 17.1$ Å, $5b = 14.3$ Å, $4b = 11.4$ Å; for the screw, $\sqrt{3}b = 4.95$ Å, $2\sqrt{3}b = 9.9$ Å.

	Edge	Screw	Ref.
Al–Mg	17.1	4.95	this study
	15.7		[8]
	~10–20	~8–16	[21]
Al–Li	11.4	9.9	This study
Al–Cu	17.1	4.95	This study
	15.7		
Al–Si	14.3	4.95	This study
	15.7		[8]
Al–Cr	17.1	4.95	This study
	17.1		[8]
Al–Fe	17.1	4.95	This study
	17.1		[8]
Al–Mn	17.1	4.95	This study
	18.6		[8]

screw dislocation has a higher line tension which does not favor a larger bow-out distance.

Numerical values of the energy barrier against dislocation motion in a solid solution with randomly distributed solute atoms, $\Delta E_b/c^{1/3}$, and the critical resolved shear stress $\tau_0/c^{2/3}$ at 0 K as predicted in this study are compared in Table 5 with predictions obtained from previous studies [7,8]. Given the different methods of obtaining the dislocation–solute interaction energy employed in this study and the previous theoretical studies, a reasonable agreement is achieved. Another comparison which should be made is the one between volume misfit parameters used in this study and those used in Ref. [7,8]. The volume misfit parameters are derived in different ways in these two studies. In this study, the volume misfit parameter is obtained

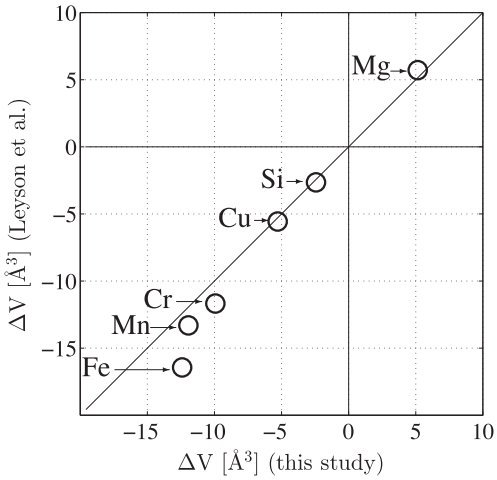

Fig. 11. Comparison of the extra volume introduced by the solute atom (ΔV) obtained in this study (Eqs. (6) and (7)) and in Ref. [8]. In Ref. [8], ΔV is evaluated by $\Delta V = \left(\frac{1}{B_{Al}} \times \frac{dP}{dc}\right) c_{1sol}$, where B is the bulk modulus of pure Al; c is the concentration; c_{1sol} is the concentration of one solute in the supercell; and P is the pressure. The pressure is calculated by using DFT under the following simulation setup: (i) the average atomic volume of the employed supercell with a single or multiple solute atoms is the same as that of pure Al; (ii) during the simulation, only the internal atomic relaxation is allowed, and the volume and the shape of the supercell is maintained; (iii) the pressure calculation is conducted on multiple supercells and multiple concentrations.

Table 5. The extra volume (ΔV, see Eq. (6) for this study) and the misfit parameter (ε_b and ε_s) of various solute elements in Al, and the predicted $\Delta E_b/c^{1/3}$ (in eV) and $\tau_0/c^{2/3}$ (in MPa) at 0 K. The line tensions of the edge and screw dislocation in pure Al in this study are 0.43 and 1.58 eV/Å, respectively, obtained by using isotropic linear elasticity theory [20], while it is calculated by using the EAM for the edge in Refs. [7,8], that their respective values are 0.25 [7] and 0.47 eV/Å [8].

	ΔV [Å^3]	ε_b	ε_s	Edge		Screw		Ref.
				$\Delta E_b/c^{1/3}$	$\tau_0/c^{2/3}$	$\Delta E_b/c^{1/3}$	$\tau_0/c^{2/3}$	
Al–Mg	5.15	0.104	−0.38	3.96	274	1.44	411	This study
	5.7			3.29	422			[7]
	5.71			4.06	342			[8]
Al–Li	−0.35	−0.007	−0.68	1.47	128	0.97	185	This study
Al–Cu	−5.29	−0.107	0.22	4.01	280	1.44	411	This study
	−5.6			3.32	430			[7]
	−5.57			4.10	348			[8]
Al–Si	−2.43	−0.049	−0.53	2.25	152	1.06	222	This study
	−2.6			2.09	170			[7]
	−2.65			2.58	137			[8]
Al–Cr	−9.93	−0.201	0.49	6.10	648	2.20	957	This study
	−11.7			5.39	871			[7]
	−11.68			6.65	705			[8]
Al–Mn	−11.94	−0.242	0.84	6.94	840	2.52	1257	This study
	−13.31			7.53	711			[8]
Al–Fe	−12.41	−0.251	0.96	7.14	888	2.60	1338	This study
	−16.44			8.2	1072			[8]

Table 6. Comparison between theoretical predicted and the experimental determined τ_0 of a few Al–X alloys at 78, 198 and 263 K. The theoretical predictions are from this study (TS) and the study by Leyson et al. [8]. The experiments are from Refs. [62,63]. Note that the experimental τ_0 was obtained by dividing the tensile yield stress of polycrystals in Refs. [62,63] by the Taylor's factor, 3.06, assuming a random texture. The concentrations in parentheses indicate the concentration of Fe. The predicted τ_0 in parentheses uses the experimentally determined quantities of Fe, $\Delta E_b/c^{\frac{1}{3}} = 28.8$ eV and $\tau_0/c^{\frac{2}{3}} = 1.3238 \times 10^4$ MPa from Ref. [8]. Note that all the predicted values are for edge dislocations.

Solute element	c [%]	τ_0 at 78 K [MPa]		
		Theory (TS)	Exp.	theory [8]
Mg	0.444	5.0	6.7	6.1
	0.810	8.0	11.2	9.6
Mn	0.123	6.8	6.8	5.7
	0.246	11.6	9.4	9.6
	0.494	19.6	14.4	16.0
Fe	7.7×10^{-4}	0.06	3.59	0.03
	16.9×10^{-4}	0.14	5.46	0.17
	43.5×10^{-4}	0.39	10.92	0.53
Cr–(Fe)	0.073-(10×10^{-4})	4.8(7.6)	7.8	3.7(6.5)
	0.302-(12×10^{-4})	14.2(16.6)	16.4	10.8(12.9)
Cu–(Fe)	0.090-(12×10^{-4})	2.1(6.0)	4.0	1.8(4.1)
	1.650-(50×10^{-4})	20.0(28.2)	28.3	17.0(25.3)
		τ_0 at 198 K [MPa]		
		Theory (TS)	Exp.	
Mn	0.123	4.0	4.9	
	0.246	7.6	6.2	
	0.494	14.0	9.2	
		τ_0 at 263 K [MPa]		
		Theory (TS)	Exp.	
Mn	0.123	3.0	3.8	
	0.246	6.1	5.7	

by using Eqs. (6) and (7), where only the geometrical quantities are used, i.e. the lattice parameter. In Refs. [7,8], the volume misfit is characterized by the extra volume, and is calculated by:

$$\Delta V = \left(\frac{1}{B_{\mathrm{Al}}} \times \frac{\mathrm{d}P}{\mathrm{d}c}\right) c_{1sol} \tag{12}$$

where B is the bulk modulus of pure Al; c is the concentration; c_{1sol} is the concentration of one solute in the supercell; and P is the pressure. The pressure is calculated by using DFT in conjunction with the following simulation setup: (i) the average atomic volume of the employed supercell with a single or multiple solute atoms is the same as that used for pure Al; (ii) during the simulation, only internal atomic relaxation is allowed, while the volume and the shape of the supercell are both maintained; (iii) the pressure calculation is conducted on multiple supercells and multiple concentrations. This approach to obtaining the volume misfit suggested in Refs. [7,8] is similar to the volume misfit proposed by Eshelby [29] (also see the discussion in Section 2.2.2 regarding the volume misfit). In Fig. 11, values for ΔV obtained by using Eq. (6) are compared with those calculated by using Eq. (12). Although a general agreement is achieved, values of ΔV obtained by using Eq. (6) are lower than those by using Eq. (12) by 5–25%.

We also compare the prediction of this study and the experiments conducted by Diak et al. [62,63] together with the theoretical prediction from Refs. [7,8] shown in Table 6. Our predictions of most systems based on using the guideline maps are in good agreement with the experiments by Diak et al. [62,63], as well as with the prediction by Leyson et al. [7,8]. The predicted solid-solution strengthening effect of Fe in Al is anomalously underestimated compared to the experiments. As shown in Table 6, the experimentally determined $\tau_0/c^{\frac{2}{3}}$ is 1.3238×10^4 MPa at 0 K [62,63,8], while in this study it is predicted to be 888 MPa for the edge, and 1338 for the screw (see Table 5). This discrepancy between the prediction and the experiments is, however, unclear at the moment.

4. Summary

We introduced and applied a multiscale simulation method for predicting solid-solution strengthening effects aiming at being computationally efficient and quantitatively accurate. This approach combines the 2-D Peierls–Nabarro model and the recent solid-solution strengthening model developed by Leyson et al. [7–9]. In this study, we focus on Al binary solid solutions.

The accuracy of this approach is exemplified by comparing the prediction with the experiments in Al–Mg and Al–Li binary solid solutions. A good agreement between theory and experiment is achieved when the temperature range corresponds to the one in which the dislocations are "overdamped".

Through reparametrization, two guideline maps of the volume parameter, ε_b, and the slip misfit parameter, ε_s against (i) the critical resolved shear stress, τ_0 at 0 K, and (ii) the energy barrier against the dislocation motion in a solid solution with randomly distributed solute atoms, ΔE_b are created. With these maps, the solid-solution strengthening effect of any solute elements in Al at 0 K and finite temperatures can be predicted by only using their misfit parameters. A good agreement is achieved between the predictions of the maps and (i) experiments [62,63]

Table A.1. Par-elastic parameters (ε_b in (A.1)), di-elastic parameters (η in (A.2)), and estimated strengthening parameters (ε in (A.3)) of Mg and Li in Al, and the experimentally determined solid-solution strengthening effect $\Delta\tau/\Delta c$ [64]. ε_b and η are determined from experimental data [45,65,46,66]. We chose 16 for α in (A.3).

	ε_b	η	ε	$\Delta\tau/\Delta c$ [MPa/at.]
Mg	0.111	−0.007	1.78	∼1000
Li	−0.007	2.127	2.13	∼220

and (ii) the previous study in which the dislocation–solute interaction energy was directly calculated by using an ab initio method [7,8].

Acknowledgments

D.M. acknowledges contributions of Prof. Phillip Eisenlohr at Michigan State University and Dr. David Steinmeitz from TARGUS Management Consulting AG who recommended to him the particle swarm optimization method. D.M. is grateful to Prof. W.A. Curtin at the École Polytechnique Fédéral de Lausanne for fruitful discussion about the solid-solution solution strengthening model during his visit to Max-Planck Insitut für Eisenforschung, Düsseldorf, Germany. D.M. also appreciates Dr. G.P.M. Leyson for reading the manuscript and giving insightful comments. M.F. acknowledges financial support from the Academy of Sciences of the Czech Republic through the Fellowship of Jan Evangelista Purkyně.

Appendix A. Estimating solid-solution strengthening of Mg and Li in Al by using linear elasticity theory

A very simple way of estimating the solid-solution strengthening is to use the par-elastic and di-elastic parameters [1–3,28]:

$$\text{par-elastic}: \quad \varepsilon_b = \left(\frac{1}{a}\frac{da}{dc}\right)_{c=0} \tag{A.1}$$

$$\text{di-elastic}: \quad \eta = \left(\frac{1}{G}\frac{dG}{dc}\right)_{c=0} \tag{A.2}$$

where a is the lattice parameter; G is the shear modulus; and c is the atomic fraction of the solute element. These two parameters are then used to calculate the strengthening parameter according to Labusch [14,15]:

$$\varepsilon = \left(\eta^2 + \alpha^2\varepsilon_b^2\right)^{\frac{1}{2}} \tag{A.3}$$

where $\alpha = 16$ for edge dislocations, and $\alpha = 3$ for screw dislocations. ε in Eq. (A.3) has proved to be useful for estimating the solid-solution strengthening, such as in Cu and Au solid solutions [58,59]. It does, however, fail to predict the solid-solution strengthening of Mg and Li in Al. In Table A.1, the strengthening parameter, ε, suggests that the solid-solution strengthening capability of Li in Al is higher than that of Mg, but experimental observations [64] show that the strengthening effect of Mg is roughly 5 times of Li.

References

[1] N.F. Mott, F.R.N. Nabarro, Proc. Phys. Soc. 52 (1940) 86–89.
[2] R.L. Fleischer, Acta Metall. 9 (1961) 996–1000.
[3] R.L. Fleischer, Acta Metall. 11 (1963) 203–209.
[4] S. Vannarat, M.H.F. Sluiter, Y. Kawazoe, Phys. Rev. B 64 (2001) 224203.
[5] J. Zander, R. Sandström, L. Vitos, Comput. Mater. Sci. 41 (2007) 86–95.
[6] H. Zhang, B. Johansson, R. Ahuja, L. Vitos, Comput. Mater. Sci. 55 (2012) 269–272.
[7] G.P.M. Leyson, W.A. Curtin, L.G. Hector Jr., C.F. Woodward, Nat. Mater. 9 (2010) 750–755.
[8] G.P.M. Leyson, L. Hector Jr., W. Curtin, Acta Mater. 60 (2012) 3873–3884.
[9] G.P.M. Leyson, L. Hector Jr., W. Curtin, Acta Mater. 60 (2012) 5197–5203.
[10] J.A. Yasi, L.G. Hector Jr., D.R. Trinkle, Acta Mater. 58 (2010) 5704–5713.
[11] L. Romaner, C. Ambrosch-Draxl, R. Pippan, Phys. Rev. Lett. 104 (2010) 195503.
[12] G. Schoeck, Philos. Mag. A 81 (2001) 1161–1176.
[13] G. Schoeck, Mater. Sci. Eng.: A 400–401 (2005) 7–17.
[14] R. Labusch, Phys. Status Solidi (b) 41 (1970) 659–669.
[15] R. Labusch, Acta Metall. 20 (1972) 917–927.
[16] M. Zaiser, Philos. Mag. A 82 (2002) 2869–2883.
[17] J. Friedel, Dislocations, Pergamon Press, Oxford, 1961.
[18] R.L. Fleischer, in: Donald Peckner (Ed.), The Strengthening in Metals, Reinhold Press, New York, 1964, pp. 93–140.
[19] G.P.M. Leyson, W.A. Curtin, Philos. Mag. 93 (2013) 2428–2444.
[20] U.F. Kocks, A.S. Argon, M.F. Ashby, Thermodynamic and Kinetics of Slip, vol. 19, Pergamon Press, Oxford, 1975.
[21] D.L. Olmsted, L.G. Hector Jr., W. Curtin, J. Mech. Phys. Solids 54 (2006) 1763–1788.
[22] J. Kennedy, R. Eberhart, Proceedings., IEEE International Conference on Neural Networks, 1995, vol. 4, 1995, pp. 1942–1948.
[23] C. Woodward, D.R. Trinkle, L.G. Hector Jr., D.L. Olmsted, Phys. Rev. Lett. 100 (2008) 045507.
[24] W. Höllerbauer, H.P. Karnthaler, Beitr. Elektonenmicr. Direktabb. Oberfl. 14 (1981) 361.
[25] G. Schoeck, Mater. Sci. Eng. A 333 (2002) 390–396.
[26] J.P. Hirth, J. Lothe, Theory of Dislocations, second ed., Krieger Publishing Company, Basel, 2006.
[27] A.V. Hershey, J. Appl. Mech.-Trans. ASME 21 (1954) 236–240.
[28] A. Cottrell, in: Report on Conference of the Strength of Solids, Physical Society, London, 1948, pp. 30–37. Conference on the Strength of Solids, 1947, London, UK.
[29] J. Eshelby, in: F. Seitz, D. Turnbull (Eds.), Solid State Physics-Advances in Research and Applications, Solid State Physics, vol. 3, Academic Press, New York, 1956, pp. 79–144.
[30] E. Clouet, Acta Mater. 54 (2006) 3543–3552.
[31] E. Clouet, S. Garruchet, H. Nguyen, M. Perez, C.S. Becquart, Acta Mater. 56 (2008) 3450–3460.
[32] Y. Hanlumyuang, P. Gordon, T. Neeraj, D. Chrzan, Acta Mater. 58 (2010) 5481–5490.
[33] D.J. Bacon, D.M. Barnett, R.O. Scattergood, Prog. Mater. Sci. 23 (1980) 51–262.
[34] G. Kresse, J. Furthmüller, Comput. Mater. Sci. 6 (1996) 15–50.
[35] G. Kresse, D. Joubert, Phys. Rev. B 59 (1999) 1758–1775.
[36] J.P. Perdew, K. Burke, M. Ernzerhof, Phys. Rev. Lett. 77 (1996) 3865–3868.
[37] P.E. Blöchl, Phys. Rev. B 50 (1994) 17953–17979.
[38] H.J. Monkhorst, J.D. Pack, Phys. Rev. B 13 (1976) 5188–5192.
[39] M. Methfessel, A.T. Paxton, Phys. Rev. B 40 (1989) 3616–3621.
[40] F. Birch, J. Appl. Phys. 9 (1938) 279–288.
[41] F. Birch, Phys. Rev. 71 (1947) 809–824.
[42] P. Söderlind, Phys. Rev. B 48 (1993) 5844.
[43] B. Grabowski, T. Hickel, J. Neugebauer, Phys. Rev. B 76 (2007) 024309.
[44] G.N. Kamm, G.A. Alers, J. Appl. Phys. 35 (1964) 327–330.

[45] J. Murray, J. Phase Equilib. 3 (1982) 60–74, 10.1007/BF02873413.
[46] A. McAlister, J. Phase Equilib. 3 (1982) 177–183.
[47] X.-Z. Wu, R. Wang, S.-F. Wang, Q.-Y. Wei, Appl. Surf. Sci. 256 (2010) 6345–6349.
[48] Y. Qi, R.K. Mishra, Phys. Rev. B 75 (2007) 224105.
[49] H. Asada, R. Horiuchi, H. Yoshinaga, S. Nakamoto, Trans. Jpn. Inst. Met. 8 (1967) 159–167.
[50] Y. Miura, S. Nishitani, M. Furukawa, M. Nemoto, in: P.O. Kettunen, T.K. Lepisto, M.E. Lehtonen (Eds.), Proceedings of the Eighth International Conference on Strength of Metals and Alloys, Vol. 2, Pergamon Press, Oxford, 1988, p. 995.
[51] H.M. Tensi, P. Dropmann, H. Borchers, Z. Metall. 61 (1970) 518–524.
[52] D. Caillard, J. Martin, Thermally Activated Mechanisms in Crystal Plasticity, Pergamon Materials Series, vol. 8, Elsevier Science, 2003, pp. 73–81.
[53] A.V. Granato, Phys. Rev. Lett. 27 (1971) 660–664.
[54] A.V. Granato, Phys. Rev. B 4 (1971) 2196–2201.
[55] A. Akhtar, E. Teghtsoonian, Philos. Mag. 25 (1972) 897–916.
[56] W.A. Curtin, D.L. Olmsted, L.G. Hector Jr., Nat. Mater. 5 (2006) 875–879.
[57] V.P. Podkuyko, V.V. Pustovalov, Fiz. Met. Metall. 39 (1975) 852–860.
[58] P. Kratochvíl, E. Neradová, Czech. J. Phys. 21 (1971) 1273–1278.
[59] P. Jax, P. Kratochvil, P. Haasen, Acta Metall. 18 (1970) 237–245.
[60] D. Ma, M. Friák, J. von Pezold, D. Raabe, J. Neugebauer, Ab-initio study of compositional trends in solid solution strengthening in metals with low Peierls stress (to be submitted).
[61] M.J. Besnus, A. Herr, A.J.P. Meyer, J. Phys. F: Met. Phys. 5 (1975) 2138–2147.
[62] B. Diak, S. Saimoto, Mater. Sci. Eng.: A 234–236 (1997) 1019–1022.
[63] B. Diak, K. Upadhyaya, S. Saimoto, Prog. Mater. Sci. 43 (1998) 223–363.
[64] B. Noble, S. Harris, K. Dinsdale, Met. Sci. 16 (1982) 425–430.
[65] C. Gault, A. Dauger, P. Boch, Phys. Status Solidi (a) 43 (1977) 625–632.
[66] W. Müller, E. Bubeck, V. Gerold, in: C. Baker, P.J. Gregson, S.J. Harris, C.J. Peel (Eds.), Aluminium–Lithium Alloys III, Proceedings of the Third International Aluminium–Lithium Conference Sponsored and Organized by the Institute of Metals, 1986, pp. 435–441.